

On the effect of isotropic and anisotropic dissipative response functions with associated and non-associated flow on the inelastic behaviour of polymeric composites.

S. G. Nagaraja^{a,1}, T. Antretter^a and C. Schuecker^b

^a Chair of Mechanics, Department of Physics, Mechanics and Electrical Engineering, Montanuniversitaet Leoben, Franz-Josef-Strasse 18/III, 8700 Leoben, Austria.

^b Chair of Designing Plastics and Composite Materials, Department of Polymer Engineering and Science, Montanuniversitaet Leoben, Otto Gloeckel-Strasse 2, 8700 Leoben, Austria.

Abstract

This article investigates the effect of using isotropic and anisotropic plastic response functions in the analysis of the elastic-plastic response of unidirectional fibre composites on the meso-scale. Three model problems that use a Drucker-Prager-type pressure-dependent yield function are considered to simulate the non-linearities exhibited by a composite material. A further core ingredient is the analysis of a canonical and non-conventional constitutive structure, with respect to associated and non-associated flow response, where the use of latter is motivated by the physical inconsistencies induced by the former under shear dominated loads. These models are evaluated quantitatively by comparison to experimental data.

Keywords: Anisotropy, plasticity, fibre-reinforced composites, associative and non-associative flow rules.

1. Introduction.

Polymeric matrix composites have attracted wide attention in recent years due to their superior mechanical properties such as strength, stiffness and fatigue resistance, among others. They are increasingly popular in the aerospace industry, automotive sector and civil engineering applications. The growing demand for polymeric matrix composites in these applications necessitates a comprehensive understanding and accurate modelling of their complex behaviour under various loading conditions. The predictive modelling of such composites is thus essential for structural integrity, design and optimisation of advanced engineering structures. Experimental investigations pertaining to the non-linear behaviour of polymeric composites are documented in [1–3], among others. It has been observed that the material response in the fibre direction remains essentially elastic up to failure, whereas the response to shear and transverse directions is non-linear and inelastic. Recent research [4, 5] additionally implies that under shear dominated loads, considerable irreversible strains develop that can be attributed to plasticity in the matrix [6]. As industries look for more lightweight, sustainable and efficient materials, the demand for thermoplastic matrix composites such as polyether ether ketone (PEEK) is

¹corresponding author. Tel.:+43 3842 402 4019

E-mail address: swaroop.gaddikere-nagaraja@unileoben.ac.at

URL: <https://mechanik.unileoben.ac.at/>

growing rapidly. Therefore, precise constitutive relations that account for the elastic-plastic behaviour of polymeric composites are essential to accurately predict the damage onset and failure of composite materials. Theoretical frameworks for the description of anisotropic plasticity with an emphasis on fibre-reinforced composites are well established in the literature, see [7–10] for the micro-mechanics based approach, [11–17] for the continuum based approach and [18, 19] for alternative formulations using the concept of mapped tensors. Though the micro-mechanical approach gives a better understanding of reasons behind the experimentally observed behaviour, it comes at a cost where higher number of coefficients are required for the description of material response, namely the constituent properties that are unavailable. Hence, attention is focussed on the latter two approaches in the present work.

The essential aspect of modelling the elastic-plastic behaviour of fibre-reinforced composites is the choice of the plastic response functions, i.e., *isotropic* or *anisotropic* dissipative functions. Isotropic dissipative functions provide a simplified analysis and are computationally efficient [20–22], however they often lead to inaccurate predictions under realistic and complex biaxial loading conditions. On the other hand, anisotropic dissipative functions [23, 24] offer a more realistic representation of the inelastic response under realistic loading conditions [25–28]. Despite this, the increased computational complexity (higher number of coefficients which must be obtained experimentally) poses significant challenges for practical implementation. A further essential aspect is the selection of *flow rules* which play a crucial role in modelling the physical behaviour of polymeric composites. Flow rules determine the direction of the plastic deformation within the material [29] and are categorised as *associative* and *non-associative flow rules*. Associative flow rules, also known as normality rules, enforce the direction of plastic flow to be perpendicular to the yield surface. With respect to polymeric composites, it is seen from [16, 28] that the predictions of associative flow rules are in excellent agreement with the experimental results under complex loading scenarios. Nevertheless, full complexity of the mechanical behaviour of the considered polymeric composite is not reproduced. An argument in [30] suggests that a non-associative flow rule must be considered in order to eliminate the physical inconsistency caused by the associated flow rules under shear dominated loads, which has been investigated and reported in the present work. A Non-associative flow rule relaxes the constraint that the plastic flow direction must be normal to the yield surface [31]. This flexibility offers additional features, such as a purely deviatoric flow rule in presence of a pressure-dependent yield function, to be incorporated in the modelling framework.

The goal of this paper is to briefly outline a thermodynamically consistent formulation of anisotropic plasticity for fibre-reinforced composites, and investigate in detail the effect of aforementioned modelling choices on the non-linear inelastic behaviour of composites. In a first step, elements of infinitesimal plasticity theory are introduced that builds the necessary background for the subsequent derivations. This is followed by a brief discussion on the general form of the energetic and dissipative response functions based on representation theorems. Next, three continuum based models are presented to simulate the non-linearities exhibited by the composite. The first model is a modified Drucker-Prager-type model, formulated following [22], in which the classical isotropic Drucker-Prager-type pressure-dependent isotropic yield criterion is modified for use with unidirectional composites. This is followed by a second model, which is a modified version of the model proposed by Car, Oller and Oñate [18, 19]. It assumes the existence of a fictitious isotropic space where a mapped problem is solved. The third model is an extension of Model-I into

an *anisotropic* form using representation theorems, discussed in [16, 17]. A further key aspect is the qualitative and quantitative evaluation of the aforementioned models by comparison to experimental data. Concluding remarks appear in the end.

2. Fundamentals of infinitesimal strain plasticity.

The infinitesimal plasticity theory [32, 33], based on the additive decomposition of the total strain into elastic and plastic parts, allows for the existence of a symmetric second-order plastic strain tensor $\boldsymbol{\varepsilon}^p$ as an internal variable. In addition, it also allows for the existence of hardening variables, which in the present work are a symmetric second-order tensor $\boldsymbol{\alpha}$ and a scalar α , characterising kinematic and isotropic hardening respectively. These variables allow for the definition of a scalar-valued energetic potential as

$$\psi = \psi(\boldsymbol{\varepsilon} - \boldsymbol{\varepsilon}^p, \boldsymbol{\alpha}, \alpha) = \frac{1}{2} \|\boldsymbol{\varepsilon} - \boldsymbol{\varepsilon}^p\|_{\mathbb{E}}^2 + \frac{1}{2} \|\boldsymbol{\alpha}\|_{\mathbb{H}}^2 + \frac{h}{n+1} (\bar{\alpha} + \alpha)^{n+1}, \quad (1)$$

where $\|\cdot\|_{(\mathbb{E}, \mathbb{H})}^2 = \langle \cdot, \cdot \rangle_{(\mathbb{E}, \mathbb{H})}$, with $\langle \cdot, \cdot \rangle$ denoting the inner product, $\boldsymbol{\varepsilon} = \nabla_{\text{Sym.}} \mathbf{u}$ is the total strain tensor defined by the symmetric part of the displacement gradient, \mathbb{E} and \mathbb{H} are fourth-order symmetric anisotropic elastic modulus and kinematic hardening modulus tensors, respectively. The parameters h and n denote the isotropic hardening modulus and exponent, respectively, while $\bar{\alpha}$ denotes prestrain which is necessary for numerical reasons and is set to a very low value such that it has negligible effect on the results [16].

The closed form expressions for the stress tensor and driving forces associated with the potential ψ are obtained by the Coleman-Noll argument [34, 35] as

$$\begin{aligned} \boldsymbol{\sigma} &= +\partial_{(\boldsymbol{\varepsilon} - \boldsymbol{\varepsilon}^p)} \psi = \mathbb{E} : (\boldsymbol{\varepsilon} - \boldsymbol{\varepsilon}^p), \\ \boldsymbol{\beta} &= -\partial_{\boldsymbol{\alpha}} \psi = -\mathbb{H} : \boldsymbol{\alpha}, \\ \beta &= -\partial_{\alpha} \psi = -h(\bar{\alpha} + \alpha)^n. \end{aligned} \quad (2)$$

Next, as a main characteristic of the elastic-plastic material response, an elastic domain \mathcal{S} is assumed, defined by

$$\mathcal{S} = \{(\boldsymbol{\sigma}, \boldsymbol{\beta}, \beta) \in \mathbb{R}^{6+6+1} \mid \chi(\boldsymbol{\sigma}, \boldsymbol{\beta}, \beta) \leq 0\}, \quad (3)$$

where $\chi = \chi(\boldsymbol{\sigma}, \boldsymbol{\beta}, \beta)$ is the yield function in the space of admissible driving forces. The yield function is of the generalised Drucker-Prager-type, and takes the form

$$\chi = \kappa p + \|\boldsymbol{\Sigma}\|_{\mathbb{P}} - \sqrt{\frac{2}{3}} [y_0 - \beta] + \frac{b}{2} \|\boldsymbol{\beta}\|_{\mathbb{Q}}^2 \quad \text{with} \quad \boldsymbol{\Sigma} = \boldsymbol{\sigma} + \boldsymbol{\beta}, \quad (4)$$

where $\|\cdot\|_{\mathbb{P}} = \sqrt{\langle \cdot, \cdot \rangle_{\mathbb{P}}}$, κ is the coefficient of the hydrostatic pressure, $p = \frac{1}{3} \text{tr}[\boldsymbol{\Sigma}]$ is the hydrostatic pressure in terms of the effective stress tensor $\boldsymbol{\Sigma}$, y_0 characterises the initial threshold yield stress, b governs the non-linearity of kinematic hardening, and $\{\mathbb{P}, \mathbb{Q}\}$ are symmetric fourth-order deviatoric Hill-type tensors.

Taking into account Eqns. (1) and (4), the generalised normality condition [36–38] yields

the flow rule and rate equations for the hardening variables as

$$\begin{aligned}\dot{\boldsymbol{\varepsilon}}^p &= \lambda \partial_{\boldsymbol{\sigma}} \chi = \lambda \left\{ \frac{\kappa}{3} \mathbf{1} + \frac{\mathbb{P} : \boldsymbol{\Sigma}}{\|\boldsymbol{\Sigma}\|_{\mathbb{P}}} \right\} \\ \dot{\boldsymbol{\alpha}} &= \lambda \partial_{\boldsymbol{\beta}} \chi = \lambda \left\{ \frac{\kappa}{3} \mathbf{1} + \frac{\mathbb{P} : \boldsymbol{\Sigma}}{\|\boldsymbol{\Sigma}\|_{\mathbb{P}}} + b \mathbb{Q} : \boldsymbol{\beta} \right\} , \\ \dot{\alpha} &= \lambda \partial_{\beta} \chi = \lambda \sqrt{\frac{2}{3}} = \sqrt{\frac{2}{3}} \|\dot{\boldsymbol{\varepsilon}}^p\|\end{aligned}\quad (5)$$

where λ denotes the amount of the plastic flow and $\mathbf{1}$ is the second-order identity tensor. Additionally, the rate equations (5) are supplemented by Karush-Kuhn-Tucker-type loading-unloading conditions such that

$$\lambda \geq 0, \quad \chi \leq 0 \quad \text{and} \quad \lambda \chi = 0 , \quad (6)$$

from which the amount of the plastic flow λ can be computed. In view of the fact that the rates of the internal variables are normal to the yield surface ($\chi = 0$), evolution laws in Eqn. (5) are referred to as associated flow rules.

For a non-associated flow response, where the canonical normal directions of the evolution equations (5) do not characterise the real material response, the constitutive response is modified by introducing an additional function ϕ , henceforth referred to as the plastic flow potential. It is assumed to be of the same form as the yield function but with a different set of governing material coefficients [31] such that

$$\phi = \tilde{\kappa} p + \|\boldsymbol{\Sigma}\|_{\mathbb{P}} - \sqrt{\frac{2}{3}} [\tilde{y}_0 - \beta] + \frac{\tilde{b}}{2} \|\boldsymbol{\beta}\|_{\mathbb{Q}}^2 , \quad (7)$$

where $\tilde{\kappa}, \tilde{y}_0, \tilde{b} \neq \kappa, y_0, b$. Consequently, the flow rule and the rate equations for the hardening variables take the form

$$\begin{aligned}\dot{\boldsymbol{\varepsilon}}^p &= \lambda \partial_{\boldsymbol{\sigma}} \phi = \lambda \left\{ \frac{\tilde{\kappa}}{3} \mathbf{1} + \frac{\mathbb{P} : \boldsymbol{\Sigma}}{\|\boldsymbol{\Sigma}\|_{\mathbb{P}}} \right\} \\ \dot{\boldsymbol{\alpha}} &= \lambda \partial_{\boldsymbol{\beta}} \phi = \lambda \left\{ \frac{\tilde{\kappa}}{3} \mathbf{1} + \frac{\mathbb{P} : \boldsymbol{\Sigma}}{\|\boldsymbol{\Sigma}\|_{\mathbb{P}}} + \tilde{b} \mathbb{Q} : \boldsymbol{\beta} \right\} . \\ \dot{\alpha} &= \lambda \partial_{\beta} \phi = \lambda \sqrt{\frac{2}{3}}\end{aligned}\quad (8)$$

Note that Eqn. (8) replaces the normality rules in Eqn. (5) though the loading-unloading conditions remain unchanged.

Remark 1. The framework of infinitesimal plasticity discussed so far, assumes a *rate-independent* setting such that the material behaviour will not qualitatively change for varying load rates $\dot{\boldsymbol{\varepsilon}}$. To account for rate-dependency, one can use the classical *rate-dependent* formulation of Perzyna-type [39, 40], which yields the plastic multiplier as

$$\lambda = \frac{1}{\eta} (\chi^+) \quad \text{with} \quad (\chi^+) := \frac{1}{2} (\chi + |\chi|) , \quad (9)$$

where $\eta \in (0, \infty)$ is the penalty parameter that characterises time-dependent viscous plastic flow and (χ^+) denotes a monotonically increasing ramp function [32, 41]. Equation

(9) is known as the *pseudo-consistency condition* which yields the rate-dependent λ in terms of viscosity η and the ramp function (χ^+). The strain-rate sensitivity of polymeric composites, particularly the shear and compressive response of AS4/PEEK is documented in [3], where it is seen that the change in elastic modulus is relatively small, whereas, for the inelastic regime, both the shear and compressive stress increases significantly with the strain rate. This phenomenon can be captured with the aid of Eqn. (9) for the present case. A rate-dependent viscoplastic formulation, cf. [17], offers additional flexibility for the choice of the slope ($\kappa/\tilde{\kappa}$) of pressure dependency, which should be rather low as pointed out in [16].

3. Transversely isotropic system \mathcal{C} generated by $(\mathbf{Q}_{\parallel\mathbf{a}}, \mathbf{Q}_{\perp\mathbf{a}}^\pi)$.

In this section, an explicit form of the scalar-valued energetic potential and the yield function is derived for the transversely isotropic symmetric group with the aid of representation theorems [42]. From a continuum viewpoint, a composite is usually characterised by two different symmetry groups based on their inherent micro-structure. If the material is reinforced by fibres in one direction, then the composite has only a single preferred direction and is characterised by the *transversely isotropic* symmetry group. Typical example is a unidirectional fibre-reinforced composite. It is also conceivable for a composite material to be reinforced by fibres in more than one direction, such as a woven fabric that has fibres aligned in two perpendicular directions. Such materials belong to the *orthorhombic* symmetry group and are characterised by the existence of two preferred directions. Focus is purely restricted to the former symmetry group in the present work. In this regard, let \mathbf{a} be a positively oriented vector denoting the preferred direction with $\|\mathbf{a}\| = 1$. The considered symmetry group \mathcal{C} is generated by the orthogonal tensors $\mathbf{Q}_{\parallel\mathbf{a}}$ and $\mathbf{Q}_{\perp\mathbf{a}}^\pi$ which correspond to arbitrary rotations relative to the vector \mathbf{a} and about a vector perpendicular to \mathbf{a} by the angle π respectively, see [43]. A key approach to the formulation of constitutive response functions with the aid of representation theorems is the construction of isotropic tensor functions with an extended set of arguments, known as structural tensors [44]. Recall here, that the transversely isotropic symmetry group is fully characterised by a single symmetric second-order structural tensor \mathbf{m} , defined by

$$\mathbf{m} = \mathbf{a} \otimes \mathbf{a} , \quad (10)$$

where \mathbf{m} is invariant to rotations \mathbf{Q} of the symmetry group \mathcal{C} , i.e. $\mathbf{Q}\mathbf{m}\mathbf{Q}^T = \mathbf{m} \ \forall \ \mathbf{Q} \in \mathcal{C}$, see [45, 46] for details. Appealing to the representation theorems for isotropic scalar and tensor functions of two symmetric second-order tensors \mathbf{A} and \mathbf{m} , an irreducible integrity basis for the transversely isotropic symmetry group is given by

$$\mathcal{I} = \{ \text{tr}[\mathbf{A}], \text{tr}[\mathbf{A}^2], \text{tr}[\mathbf{A}^3], \text{tr}[\mathbf{m}\mathbf{A}], \text{tr}[\mathbf{m}\mathbf{A}^2] \} , \quad (11)$$

see [47–49]. Following [16, 17], the set of invariants in Eqn. (11) can be reformulated to

$$\tilde{\mathcal{I}} = \{ \tilde{I}_1, \dots, \tilde{I}_5 \} = \left\{ \text{tr}[\mathbf{m}\mathbf{A}], \text{tr}[(\mathbf{1} - \mathbf{m})\mathbf{A}], \text{tr}[\mathbf{m}\mathbf{A}^2], \text{tr} \left[\left(\frac{1}{2}\mathbf{1} - \mathbf{m} \right) \mathbf{A}^2 \right], \det[\mathbf{A}] \right\} , \quad (12)$$

where the first two invariants in Eqn. (12) are normal modes and the next two modes are shear. Scalar-valued constitutive functions can now be constructed by taking combinations of the invariants defined above. In particular, a *quadratic* potential Π can be written as

$$\Pi = \frac{\mu_1}{2} \tilde{I}_1^2 + \frac{\mu_2}{2} \tilde{I}_2^2 + \mu_3 \tilde{I}_1 \tilde{I}_2 + 2\mu_4 \tilde{I}_3 + 2\mu_5 \tilde{I}_4 , \quad (13)$$

where μ_{1-5} are five independent Lamé parameters required to describe the transversely isotropic response. Note that the cubic invariant \tilde{I}_5 is neglected as it is most suitable for modelling metal plasticity. The closed form expression of the fourth-order Hessian associated with the potential reads

$$\begin{aligned} \mathbb{A} = \Pi_{,AA} = & \mu_1 \mathbf{m} \otimes \mathbf{m} + \mu_2 \{(\mathbf{1} - \mathbf{m}) \otimes (\mathbf{1} - \mathbf{m})\} \\ & + \mu_3 \{ \mathbf{m} \otimes (\mathbf{1} - \mathbf{m}) + (\mathbf{1} - \mathbf{m}) \otimes \mathbf{m} \} \\ & + \mu_4 \{ (\mathbf{1} \oplus \mathbf{m}) + (\mathbf{1} \ominus \mathbf{m}) + (\mathbf{m} \oplus \mathbf{1}) + (\mathbf{m} \ominus \mathbf{1}) \} \\ & + \mu_5 \{ (\mathbf{1} \oplus \mathbf{1}) + (\mathbf{1} \ominus \mathbf{1}) - (\mathbf{1} \oplus \mathbf{m}) - (\mathbf{1} \ominus \mathbf{m}) - (\mathbf{m} \oplus \mathbf{1}) - (\mathbf{m} \ominus \mathbf{1}) \} \end{aligned} \quad (14)$$

where the identities

$$\begin{aligned} \{(\bullet) \otimes (\bullet)\}_{ijkl} &= (\bullet)_{ij}(\bullet)_{kl} \\ \{(\bullet) \oplus (\bullet)\}_{ijkl} &= (\bullet)_{ik}(\bullet)_{jl} \quad , \\ \{(\bullet) \ominus (\bullet)\}_{ijkl} &= (\bullet)_{il}(\bullet)_{jk} \end{aligned} \quad (15)$$

have been introduced. For the choice of $\mathbf{a} = [1, 0, 0]^T$, the Hessian \mathbb{A} appears in the coordinate form

$$[\mathbb{A}] = \begin{bmatrix} \mu_1 + 4\mu_4 - 2\mu_5 & \mu_3 & \mu_3 & 0 & 0 & 0 \\ & \mu_2 + 2\mu_5 & \mu_2 & 0 & 0 & 0 \\ & & \mu_2 + 2\mu_5 & 0 & 0 & 0 \\ & & & \mu_4 & 0 & 0 \\ & & & & \mu_4 & 0 \\ \text{Sym.} & & & & & \mu_5 \end{bmatrix} \quad , \quad (16)$$

where it is seen that the fourth-order tensor \mathbb{A} satisfies major and minor symmetries, i.e.,

$$\mathbb{A}_{ijkl} = \mathbb{A}_{jikl} = \mathbb{A}_{ijlk} = \mathbb{A}_{klij} \quad . \quad (17)$$

4. Continuum formulation.

In this section, simple models of anisotropic plasticity are discussed which can be used for the analysis of infinitesimal elastic-plastic deformation of fibre-reinforced composites. Starting with the elastic response functions, use is made of Eqn. (16) to first define the scalar-valued energetic function. Based on the elements of infinitesimal plasticity theory introduced in Section 2, three models chosen from the literature are presented to simulate the non-linearities exhibited by the composite. The first model is a modified Drucker-Prager model (Model-I), formulated following [22], in which the classical Drucker-Prager-type pressure-dependent isotropic yield criterion is modified for use with fibre-reinforced composites. Here, only the volumetric-isochoric decomposition of the stress tensor is considered. This is followed by a second model, which is a modified version of the model proposed by Car, Oller and Oñate [18, 19] (Model-II). It assumes the existence of a fictitious isotropic space where a mapped problem is solved. The third model (Model-III) is an extension of Model-I into an *anisotropic* form using representation theorems, discussed in [16, 17]. All the models use the classical Drucker-Prager-type yield function, mainly for the computational aspects owing to its smooth surface and numerical stability.

4.1. Elastic response functions.

Setting $\mathbb{A} = \mathbb{E}$ in Eqn. (1), the stress tensor defined in Eqn. (2)₁, is obtained in terms of the respective governing coefficients, see also [41]. Note that the Lamé parameters are identified in terms of the corresponding engineering constants using the prescription suggested in [50]. For the sake of simplicity and absence of relevant experimental data, $\mathbb{H} = \mathbb{0}$ is reasonably assumed. Next, the plastic response functions are formulated with the preceding definitions at hand.

4.2. Plastic response functions.

In the context of formulating the plastic response functions for unidirectional fibre-reinforced composites, Spencer [24] introduced a physically motivated plasticity inducing stress tensor which is obtained in an additive format from the overall stress, the hydrostatic pressure and the deviatoric fibre stress for a given fibre direction \mathbf{m} [23, 24, 43]. This is specified to the present model problems by defining a fourth-order projection tensor

$$\mathbb{P} = (\mathbf{1} \oplus \mathbf{1}) + (\mathbf{1} \ominus \mathbf{1}) - \frac{1}{3}(\mathbf{1} \otimes \mathbf{1}) - \frac{3}{2}(\mathbf{m}' \otimes \mathbf{m}') \quad \text{with} \quad \mathbf{m}' = \mathbf{m} - \frac{1}{3}\mathbf{1}, \quad (18)$$

with the following characteristics

$$\text{tr}[\mathbb{P} : \mathbf{1}] = 0 \quad \text{and} \quad \text{tr}[\mathbb{P} : \mathbf{m}] = 0. \quad (19)$$

Additionally, let p denote the hydrostatic pressure such that

$$p = \frac{1}{3} \text{tr}[(\mathbf{1} - \mathbf{m})\boldsymbol{\Sigma}]. \quad (20)$$

Note, \mathbb{P} and p in Eqns. (18) and (20), respectively, ensure a linear elastic fibre response.

4.2.1. Model-I.

Appealing to Eqns. (18) and (20), the yield function for Model-I now reads

$$\chi = \kappa p + \|\boldsymbol{\Sigma}\|_{\mathbb{P}} - \sqrt{\frac{2}{3}}[y_0 - \beta] + \frac{b}{2}\|\boldsymbol{\beta}\|_{\mathbb{Q}}^2. \quad (21)$$

The normality rules in Eqn. (5) reformulate with Eqn. (21) to

$$\begin{aligned} \dot{\boldsymbol{\epsilon}}^p &= \lambda \left\{ \frac{\kappa}{3}(\mathbf{1} - \mathbf{m}) + \frac{\mathbb{P} : \boldsymbol{\Sigma}}{\|\boldsymbol{\Sigma}\|_{\mathbb{P}}} \right\} \\ \dot{\boldsymbol{\alpha}} &= \lambda \left\{ \frac{\kappa}{3}(\mathbf{1} - \mathbf{m}) + \frac{\mathbb{P} : \boldsymbol{\Sigma}}{\|\boldsymbol{\Sigma}\|_{\mathbb{P}}} + b\mathbb{Q} : \boldsymbol{\beta} \right\}. \\ \dot{\alpha} &= \lambda \sqrt{\frac{2}{3}} \end{aligned} \quad (22)$$

For the case of non-associative plasticity, the corresponding flow rule and rate equations for the hardening variables can be obtained in a similar manner. In particular, a deviatoric flow potential is chosen following [31] as

$$\phi := \chi|_{\kappa=0} = \|\boldsymbol{\Sigma}\|_{\mathbb{P}} - \sqrt{\frac{2}{3}}[y_0 - \beta] + \frac{b}{2}\|\boldsymbol{\beta}\|_{\mathbb{Q}}^2, \quad (23)$$

based on which the evolution equations in Eqn. (8) take the form

$$\begin{aligned}\dot{\boldsymbol{\varepsilon}}^p &= \lambda \left\{ \frac{\mathbb{P} : \boldsymbol{\Sigma}}{\|\boldsymbol{\Sigma}\|_{\mathbb{P}}} \right\} \\ \dot{\boldsymbol{\alpha}} &= \lambda \left\{ \frac{\mathbb{P} : \boldsymbol{\Sigma}}{\|\boldsymbol{\Sigma}\|_{\mathbb{P}}} + b\mathbb{Q} : \boldsymbol{\beta} \right\} . \\ \dot{\alpha} &= \lambda \sqrt{\frac{2}{3}}\end{aligned}\quad (24)$$

4.2.2. Model-II.

This is a material model for fibre-reinforced composites based on the work of Car, Oller and Oñate [18, 19]. It assumes the existence of a fictitious isotropic space where a mapped problem is solved. The real and fictitious spaces are related by means of fourth-order transformation tensors which are formulated based on the available information of strengths in the respective spaces. The real anisotropic space is regarded as a homogenised composite material, while the fictitious isotropic space characterises the matrix material to which plasticity is usually restricted.

Let \mathbf{Y} and $\overline{\mathbf{Y}}$ each represent a second-order yield strength tensor for the real anisotropic space and the fictitious isotropic space, respectively. Based on the yield strength tensors, a fourth-order space transformation tensor for the stress is proposed as

$$\mathbb{M} = \frac{1}{2} \{ (\overline{\mathbf{Y}} \oplus \mathbf{Y}^{-1}) + (\mathbf{Y}^{-1} \oplus \overline{\mathbf{Y}}) \} , \quad (25)$$

which satisfies the major and minor symmetries

$$\mathbb{M}_{ijkl} = \mathbb{M}_{jikl} = \mathbb{M}_{ijlk} = \mathbb{M}_{klij} . \quad (26)$$

The fourth-order tensor \mathbb{M} relates the stress tensor and the back-stress tensor in the real and fictitious spaces as

$$\overline{\boldsymbol{\sigma}} = \mathbb{M} : \boldsymbol{\sigma} \quad \text{and} \quad \overline{\boldsymbol{\beta}} = \mathbb{M} : \boldsymbol{\beta} , \quad (27)$$

with $\boldsymbol{\sigma}$ denoting the stress tensor in the real anisotropic space, defined in Eqn. (2)₁. It should be noted here that Car, Oller and Oñate [18, 19] defined the transformation tensor as $\mathbb{M} = \overline{\mathbf{Y}} \otimes \mathbf{Y}^{-1}$, but it is slightly modified in the present work to get a compact representation of the transformation tensor. In what follows, the quantities (\cdot) and $(\overline{\cdot})$ relate to the real anisotropic and the fictitious isotropic space, respectively. Analogous to Eqn. (27), the relationship between the elastic strain in both spaces is defined by

$$(\overline{\boldsymbol{\varepsilon}} - \overline{\boldsymbol{\varepsilon}}^p) = \mathbb{N} : (\boldsymbol{\varepsilon} - \boldsymbol{\varepsilon}^p) , \quad (28)$$

which implies the non-uniqueness of elastic strain during space transformation. The fourth-order strain transformation tensor \mathbb{N} is obtained with the aid of Eqn. (27) as

$$\mathbb{N} = \overline{\mathbb{E}}^{-1} : \mathbb{M} : \mathbb{E} , \quad (29)$$

where \mathbb{E} and $\overline{\mathbb{E}}$ are the elastic modulus tensors in the real anisotropic and fictitious isotropic spaces, respectively. The fourth-order tensor \mathbb{E} includes the actual properties of the material, i.e., Eqn. (16), whereas the choice of $\overline{\mathbb{E}}$ can be mathematically arbitrary

[18, 19] but should physically represent the matrix constituent. In what follows, the governing constitutive equations of the plastic deformation process are specified in the fictitious isotropic space. Note that it is equivalent to formulate the model in either of the two spaces because of the invariance of the dissipation postulate [18]. Due to the advantages of the existing algorithms for isotropy, modelling in the fictitious isotropic space is considered here.

Starting from Eqn. (4), the yield function in the fictitious isotropic space is given by

$$\chi = \kappa \bar{p} + \|\bar{\Sigma}\|_{\bar{\mathbb{P}}} - \sqrt{\frac{2}{3}}[y_0 - \beta] + \frac{b}{2} \|\bar{\beta}\|_{\bar{\mathbb{Q}}}^2 \quad \text{with} \quad \bar{\Sigma} = \bar{\sigma} + \bar{\beta}, \quad (30)$$

where $\bar{p} = \frac{1}{3} \text{tr}[\bar{\Sigma}]$ is the hydrostatic pressure, and $\bar{\mathbb{P}}$ is the symmetric isotropic fourth-order deviatoric projection tensor given by

$$\bar{\mathbb{P}} = (\mathbf{1} \oplus \mathbf{1}) + (\mathbf{1} \ominus \mathbf{1}) - \frac{1}{3}(\mathbf{1} \otimes \mathbf{1}). \quad (31)$$

Recall here that the deviatoric fourth-order Hill-type tensor $\bar{\mathbb{Q}}$ is similar to $\bar{\mathbb{P}}$, and governs the non-linearity of kinematic hardening. The flow rule and rate equations of the hardening variables within the isotropic space are specified analogous to Eqn. (22) as

$$\begin{aligned} \dot{\bar{\epsilon}}^p &= \lambda \left\{ \frac{\kappa}{3} \mathbf{1} + \frac{\bar{\mathbb{P}} : \bar{\Sigma}}{\|\bar{\Sigma}\|_{\bar{\mathbb{P}}}} \right\} \\ \dot{\bar{\alpha}} &= \lambda \left\{ \frac{\kappa}{3} \mathbf{1} + \frac{\bar{\mathbb{P}} : \bar{\Sigma}}{\|\bar{\Sigma}\|_{\bar{\mathbb{P}}}} + b \bar{\mathbb{Q}} : \bar{\beta} \right\} . \\ \dot{\bar{\alpha}} &= \lambda \sqrt{\frac{2}{3}} \end{aligned} \quad (32)$$

Furthermore, a separate deviatoric flow potential that governs the evolution of plastic variables within the framework of non-associative plasticity is defined as

$$\phi := \chi|_{\kappa=0} = \|\bar{\Sigma}\|_{\bar{\mathbb{P}}} - \sqrt{\frac{2}{3}}[y_0 - \beta] + \frac{b}{2} \|\bar{\beta}\|_{\bar{\mathbb{Q}}}^2, \quad (33)$$

based on which the evolution equations (32) reformulate respectively to

$$\begin{aligned} \dot{\bar{\epsilon}}^p &= \lambda \left\{ \frac{\bar{\mathbb{P}} : \bar{\Sigma}}{\|\bar{\Sigma}\|_{\bar{\mathbb{P}}}} \right\} \\ \dot{\bar{\alpha}} &= \lambda \left\{ \frac{\bar{\mathbb{P}} : \bar{\Sigma}}{\|\bar{\Sigma}\|_{\bar{\mathbb{P}}}} + b \bar{\mathbb{Q}} : \bar{\beta} \right\} . \\ \dot{\bar{\alpha}} &= \lambda \sqrt{\frac{2}{3}} \end{aligned} \quad (34)$$

for the non-associative flow response. Equations (30), (32) and (34) are solved by a general elastic predictor-plastic corrector algorithm described in [33, 50], which gives the consistent update of the stress tensor, plastic strain tensor, hardening variables and the algorithmically consistent elastic-plastic tangent modulus. With these tensorial quantities

in the fictitious isotropic space at hand, the corresponding real anisotropic counterparts are obtained by a straightforward transformation as follows

$$\boldsymbol{\sigma}^{\text{ep}} = \mathbb{M}^{-1} : \bar{\boldsymbol{\sigma}}^{\text{ep}} \quad \text{and} \quad \mathbb{E}^{\text{ep}} = \mathbb{M}^{-1} : \bar{\mathbb{E}}^{\text{ep}} : \mathbb{N} . \quad (35)$$

In summary, Model-II requires the following material properties to describe the elastic-plastic response of unidirectional fibre-reinforced composite materials:

- Real anisotropic space:
 - elastic parameters μ_{1-5} ,
 - yield strength tensor \mathbf{Y} .
- Fictitious isotropic space:
 - plastic parameters $\kappa, y_0, h, \bar{\alpha}, n$ and b ,
 - yield strength tensor $\bar{\mathbf{Y}}$.

4.2.3. Model-III.

The third model (Model-III) considers an extension of the isotropic plastic response functions of Model-I into *anisotropic* forms using the representation theorems discussed in [16, 17]. Precisely, a further decomposition of \mathbb{P} in Eqn. (18) into the two shear modes associated with the symmetry group is considered. To this end, we define

$$\mathbb{P} = \mathbb{P}_1 + \mathbb{P}_2 , \quad (36)$$

where, following [43], it can be verified that

$$\mathbb{P}_1 = \frac{1}{2}[(\mathbf{1} \oplus \mathbf{m}) + (\mathbf{m} \oplus \mathbf{1}) + (\mathbf{1} \ominus \mathbf{m}) + (\mathbf{m} \ominus \mathbf{1}) - 2(\mathbf{m} \otimes \mathbf{m})] \quad \text{and} \quad \mathbb{P}_2 = \mathbb{P} - \mathbb{P}_1 . \quad (37)$$

In the equation above \mathbb{P}_1 and \mathbb{P}_2 are the in-plane and transverse shear modes. The fourth-order tensors \mathbb{Q}_1 and \mathbb{Q}_2 are obtained similar to \mathbb{P}_1 and \mathbb{P}_2 , respectively. Equation (37) allows for the definition of the yield function for Model-III, entirely analogous to [16, 17] as

$$\chi = \kappa p + \|\boldsymbol{\Sigma}\|_{(a_1\mathbb{P}_1+a_2\mathbb{P}_2)} - \left[1 - \frac{\beta}{y_{12}}\right] + \frac{1}{2}\|\boldsymbol{\beta}\|_{(b_1\mathbb{Q}_1+b_2\mathbb{Q}_2)}^2 , \quad (38)$$

see also [51], where p is the hydrostatic pressure defined in Eqn. (20). The four parameters κ, a_1, a_2 and y_{12} in the equation above govern the transversely isotropic plastic yielding. They are determined by the evaluation of the yield function (38) for two simple shear tests and one normal (compression) test, with $\beta = 0$ and $\boldsymbol{\beta} = \mathbf{0}$ [16], as

$$\kappa = \frac{1}{\sqrt{2}y_{23}} - \frac{1}{y_{22c}} , \quad a_1 = \frac{1}{y_{12}^2} \quad \text{and} \quad a_2 = \frac{1}{y_{23}^2} . \quad (39)$$

where y_{12}, y_{23} and y_{22} denote the in-plane, transverse shear and transverse compressive yield stress respectively. The remaining two parameters b_1 and b_2 in Eqn. (38) govern the non-linearity of kinematic hardening. Considering the fact that the Hessian of the squared Euclidean norm is the identity matrix which is axiomatically positive definite, the requirement for convexity of the yield surface (38) is given by $a_{1-2} \geq 0$, see also Naghdi-Trapp inequality [52–54], which is generally fulfilled by Eqn. (39).

The normality rules for Model-III follow with the aid of Eqn. (38) as

$$\begin{aligned}\dot{\boldsymbol{\varepsilon}}^p &= \lambda \left\{ \frac{\kappa}{3}(\mathbf{1} - \mathbf{m}) + \frac{(a_1 \mathbb{P}_1 + a_2 \mathbb{P}_2) : \boldsymbol{\Sigma}}{\|\boldsymbol{\Sigma}\|_{(a_1 \mathbb{P}_1 + a_2 \mathbb{P}_2)}} \right\} \\ \dot{\boldsymbol{\alpha}} &= \lambda \left\{ \frac{\kappa}{3}(\mathbf{1} - \mathbf{m}) + \frac{(a_1 \mathbb{P}_1 + a_2 \mathbb{P}_2) : \boldsymbol{\Sigma}}{\|\boldsymbol{\Sigma}\|_{(a_1 \mathbb{P}_1 + a_2 \mathbb{P}_2)}} + (b_1 \mathbb{Q}_1 + b_2 \mathbb{Q}_2) : \boldsymbol{\beta} \right\} \cdot \\ \dot{\alpha} &= \lambda \frac{1}{y_{12}}\end{aligned}\quad (40)$$

Analogous to the previous two models, a plastic flow potential that governs the non-associated flow response of Model-III can be specified as

$$\phi := \chi|_{\kappa=0} = \|\boldsymbol{\Sigma}\|_{(a_1 \mathbb{P}_1 + a_2 \mathbb{P}_2)} - \left[1 - \frac{\beta}{y_{12}} \right] + \frac{1}{2} \|\boldsymbol{\beta}\|_{(b_1 \mathbb{Q}_1 + b_2 \mathbb{Q}_2)}^2. \quad (41)$$

Consequently, the evolution equations for a non-associated flow response read

$$\begin{aligned}\dot{\boldsymbol{\varepsilon}}^p &= \lambda \left\{ \frac{(a_1 \mathbb{P}_1 + a_2 \mathbb{P}_2) : \boldsymbol{\Sigma}}{\|\boldsymbol{\Sigma}\|_{(a_1 \mathbb{P}_1 + a_2 \mathbb{P}_2)}} \right\} \\ \dot{\boldsymbol{\alpha}} &= \lambda \left\{ \frac{(a_1 \mathbb{P}_1 + a_2 \mathbb{P}_2) : \boldsymbol{\Sigma}}{\|\boldsymbol{\Sigma}\|_{(a_1 \mathbb{P}_1 + a_2 \mathbb{P}_2)}} + (b_1 \mathbb{Q}_1 + b_2 \mathbb{Q}_2) : \boldsymbol{\beta} \right\} \cdot \\ \dot{\alpha} &= \lambda \frac{1}{y_{12}}\end{aligned}\quad (42)$$

4.3. General remarks for algorithmic implementation.

The next computational aspect is the time integration of the rate equations of the models, subject to the constraint posed by the respective yield conditions. The general return method suggested in [33, 50], together with a backwards Cauchy-Euler integration scheme is used here in entire analogy. While the parameters κ , a_1 , a_2 and y_{12} are obtained from the experimental curves, the kinematic hardening parameters b_1 and b_2 are set to zero in the present work owing to absence of relevant experimental data. A recipe for the identification of material parameters associated with kinematic hardening can however be found in [55]. Furthermore, the evolution equations of all the three models characterise Armstrong-Fredrick-type non-linear kinematic hardening [56], generalised to the present case. For the choice $b = b_1 = b_2 = 0$, the models recover the well known Melan-Prager-type kinematic hardening [57], where $\boldsymbol{\alpha}$ is linear and homogeneous in $\dot{\boldsymbol{\varepsilon}}^p$ [41, 51].

In summary, two different constitutive laws are implemented for each model, namely

1. Model-I-a/Model-II-a/Model-III-a: associative pressure-dependent models, obtained by Eqns. (1) and (21)/(30)/(38).
2. Model-I-b/Model-II-b/Model-III-b: non-associative pressure-dependent models, given by Eqns. (1), (21)/(30)/(38) and (23)/(33)/(41).

TABLE 1: Material parameters for Model-I.

No.	Name	Par.	Value	Unit
1.	Longitudinal Young's modulus	E_1	130000	[MPa]
2.	Transverse Young's modulus	E_2	11000	[MPa]
3.	Longitudinal shear modulus	G_{12}	5800	[MPa]
4.	Transverse shear modulus	G_{23}	3720	[MPa]
5.	Poisson's ratio	ν_{12}	0.306	[-]
6.	Coefficient of hydrostatic pressure	κ	$0.9497^a/1.105^b$	[-]
7.	Initial yield stress	y_0	10.6	[MPa]
8.	Hardening modulus	h	237.9	[MPa]
9.	Pre-strain	$\bar{\alpha}$	1×10^{-12}	[-]
10.	Hardening exponent	n	0.249	[-]

TABLE 2: Material parameters for Model-II.

No.	Name	Par.	Value	Unit
1.	Longitudinal Young's modulus	E_1	130000	[MPa]
2.	Transverse Young's modulus	E_2	11000	[MPa]
3.	Longitudinal shear modulus	G_{12}	5800	[MPa]
4.	Transverse shear modulus	G_{23}	3720	[MPa]
5.	Poisson's ratio	ν_{12}	0.306	[-]
6.	Anisotropic space yield strength	Y_{11}	$\approx \infty$	[MPa]
7.	Anisotropic space yield strength	Y_{22}	158.6	[MPa]
8.	Isotropic space yield strength	\bar{Y}	158.6	[MPa]
9.	Coefficient of hydrostatic pressure	κ	$1.931^a/1.917^b$	[-]
10.	Initial yield stress	y_0	20.5	[MPa]
11.	Hardening modulus	h	415.7	[MPa]
12.	Pre-strain	$\bar{\alpha}$	1×10^{-12}	[-]
13.	Hardening exponent	n	0.241	[-]

TABLE 3: Material parameters for Model-III

No.	Name	Par.	Value	Unit
1.	Longitudinal Young's modulus	E_1	130000	[MPa]
2.	Transverse Young's modulus	E_2	11000	[MPa]
3.	Longitudinal shear modulus	G_{12}	5800	[MPa]
4.	Transverse shear modulus	G_{23}	3720	[MPa]
5.	Poisson's ratio	ν_{12}	0.306	[-]
6.	Transverse compressive yield stress	y_{22c}	$24.6^a/27.4^b$	[MPa]
7.	In-plane shear yield stress	y_{12}	9.41	[MPa]
8.	Transverse shear yield stress	y_{23}	10.66	[MPa]
9.	Hardening modulus	h	177.5	[MPa]
10.	Pre-strain	$\bar{\alpha}$	1×10^{-12}	[-]
11.	Hardening exponent	n	0.246	[-]

^aAssociative flow^bNon-associative flow

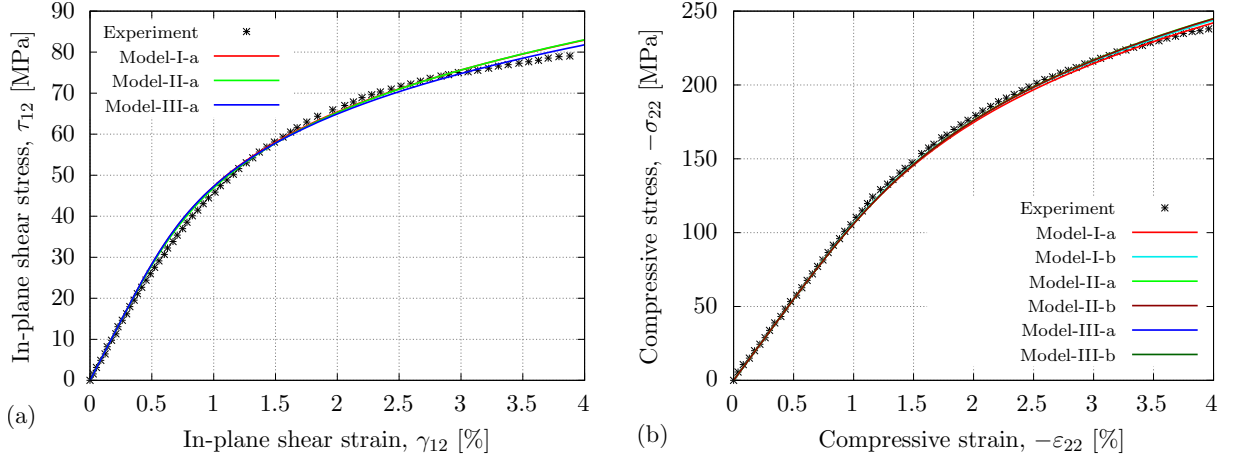


FIGURE 1: **Calibration results.** Comparison of the experimental data [3] and the three meso models responses for (a) in-plane shear and (b) transverse compression load.

5. Numerical simulations.

The proposed models are implemented as user subroutines (UMAT) in ABAQUS, a general purpose non-linear finite element program documented in [58]. The subsequent numerical simulations demonstrate the applicability and predictive capabilities of the models. In this regard, the inelastic behaviour of a certain composite which has carbon fibres reinforced in a polymer matrix (AS4/PEEK) is considered. The pertinent experimental investigations are documented in [3]. Note, that the simulations are conducted using a single hexahedral 3D continuum element (C3D8). To avoid rigid body motions, the bottom, left and rear faces are constrained in vertical, horizontal and lateral directions, respectively, for the transverse compression load. For the shear load, left face is fully constrained in all the directions while the load is applied on the lateral face. The material parameters used in the numerical simulations are listed in Tables 1–3, wherein, the elastic parameters for all the three models are taken directly from [3, 8]. Additionally, the elastic material parameters for the fictitious isotropic space in Model-II are chosen to be $E = 4100$ MPa and $\nu = 0.356$, which are the matrix properties of PEEK [3]. The plastic parameters of Model-I and Model-II are calibrated using the procedure detailed in our previous work [16], from which all the material parameters for Model-III are also taken.

5.1. Calibration for the standard load cases.

Figure 1 shows the calibration results comparing test data [3] and the three meso models for the two standard test cases, namely the in-plane and transverse compression test case. All the models reproduce the shear response and the transverse compressive response accurately, as seen in Fig. 1 (a) and (b). The experimental observations [3] and computational verifications [8, 16] are affirmative to the fact that the constitutive response must be pressure sensitive to realistically predict the non-linear behaviour of composite materials. Furthermore, it should be noted from Tables 1–3 that the coefficient of hydrostatic pressure differs slightly between associative and non-associative models.

5.2. Predictions for biaxial loads.

Next, the predictions of the three calibrated models are compared with experimental results from the literature [3] for a set of biaxial loads. Two different load paths are considered which are summarised in Table 4. For the first load path, referred to as the

TABLE 4: Summary of the load paths

Load path	No.	τ_{12}^*	$-\sigma_{22}^*$	Unit
Shear preload: $\tau_{12} \rightarrow -\varepsilon_{22}$	①	43.1	–	[MPa]
	②	56.2	–	[MPa]
	③	66.9	–	[MPa]
	④	79.5	0	[MPa]
Compression preload: $-\sigma_{22} \rightarrow \gamma_{12}$	⑤	–	50.2	[MPa]
	⑥	–	84.83	[MPa]
	⑦	–	124.1	[MPa]
	⑧	–	164.5	[MPa]
	⑨	0	242.6	[MPa]

$\tau_{12} \rightarrow -\varepsilon_{22}$ path, the specimen is first sheared to a predetermined stress level (τ_{12}^*) and it is then compressed under displacement control while the shear stress is kept constant. The final value of compressive strain is chosen to be $-\varepsilon_{22} = 4\%$. Likewise, in the second load path, referred to as the $-\sigma_{22} \rightarrow \gamma_{12}$ path, the specimen is first compressed to a desired stress level ($-\sigma_{22}^*$) and then sheared with $\gamma_{12} = 4\%$ while keeping the transverse compressive stress constant. The desired shear and compressive stress values are taken directly from [3]. Note that, the experimental investigations additionally examine non-proportional load paths, where a set of load paths with proportional increase of compressive and shear stresses is considered. A detailed comparison of models predictions and experimental data for the non-proportional load paths is documented in [16], and hence not considered here.

5.2.1. Predictions of the associated flow response.

Starting with the $\tau_{12} \rightarrow -\varepsilon_{22}$ load path, Fig. 2 shows a comparison of the model predictions with the experimental results. The graphs in the left column show the compressive responses under the shear preload along with a pure compression case. The experimental results indicate that despite the initial yielding caused by the shear preload, the compressive responses for load paths ① and ② are almost identical to ⑨, while that for ③ is somewhat lower. It can also be inferred from the experimental results that the material response first softens and then subsequently stiffens for increasing shear preloads. The graphs in the right column show the increase in shear strain caused by the compression load. It is seen that the increase is comparatively large for load path ③ although a small bump in γ_{12} can be seen at low values of σ_{22} , which can be attributed to a test artefact [3]. The compressive responses predicted by Model-I-a along with a pure compression case (load path ⑨) are shown in Fig. 2 (a). The general behaviour of softening and subsequent stiffening for increasing preloads is not captured by the model. Additionally, for shear dominated stress states (load paths ①–③), erroneous predictions of Model-I-a can be seen where tensile strain is predicted. Good qualitative agreement with the experimental response is seen in Fig. 2 (b) with the predicted shear strains being rather high. Figures 2 (c) and (d) show a comparison of Model-II-a predictions and experimental results for the $\tau_{12} \rightarrow -\varepsilon_{22}$ load path. Though there are no erroneous predictions for shear dominated loads, the general trends of experimentally observed behaviour are not captured by the model, as seen from Fig. 2 (c). For the load path ③, there is

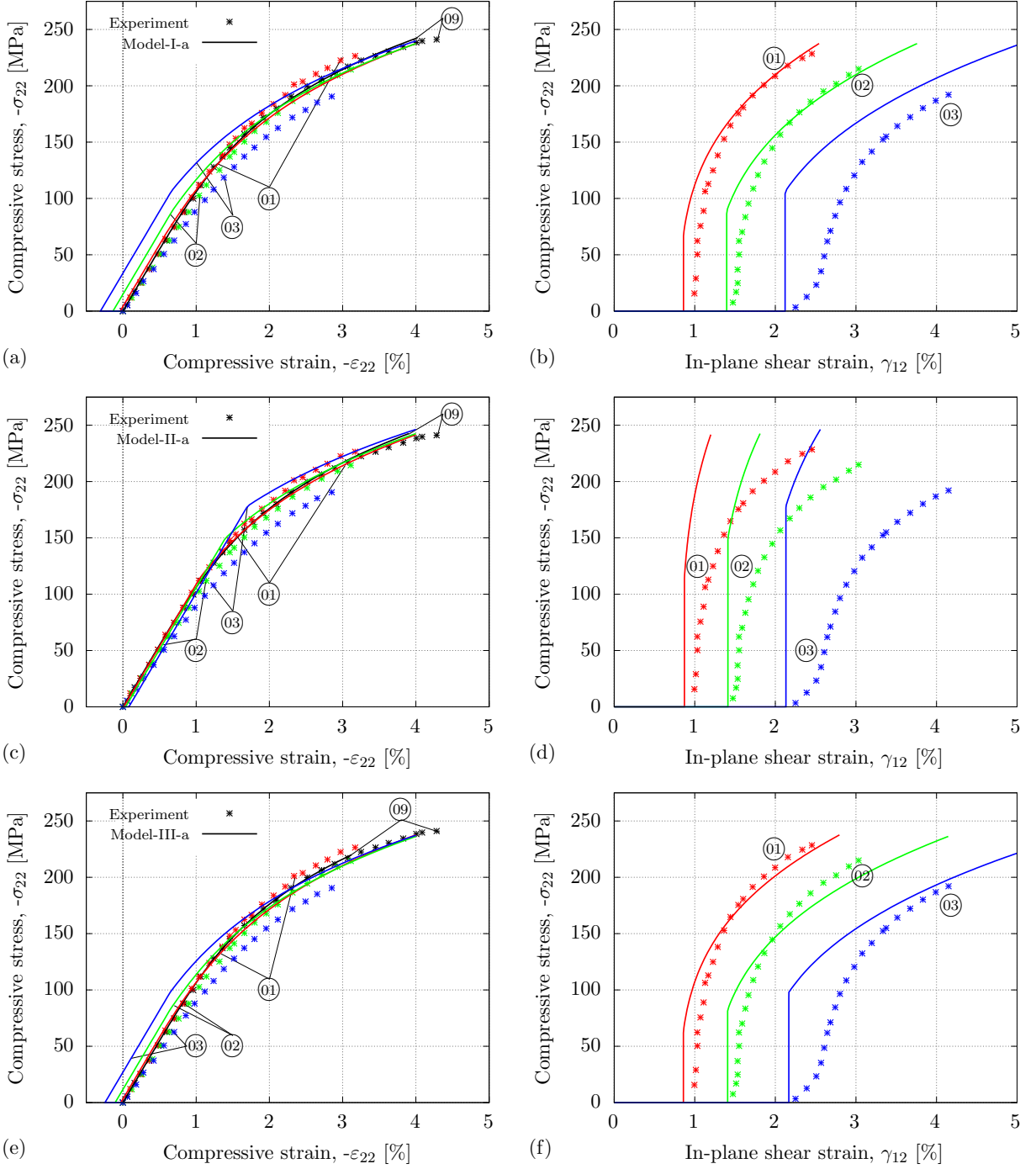


FIGURE 2: **Predictions for biaxial loads.** Comparison of the experimental and associative model responses for the $\tau_{12} \rightarrow -\varepsilon_{22}$ loading path.

an observable over-prediction by the model. In comparison with the previous case, the agreement with the experimental response is not satisfactory, as evident from Fig. 2 (d). Figures 2 (e) and (f) show the predictions of Model-III-a for the $\tau_{12} \rightarrow -\varepsilon_{22}$ load path. The use of associative flow rule induces physical inconsistencies in the response where tensile transverse strains are predicted for shear dominated stress states (load paths 02 and 03). The predicted compressive response by the model agrees well with experiments, as seen in Fig. 2 (e). Only for the highest shear preload (load path 03), the response is slightly over-predicted. The general trend of the experimental behaviour where the

material response first shifts up and then down for increasing shear preloads is also not captured by the model, though the effect is minimal. The predicted shear strains agree well with the experimental response (Fig. 2 (f)), except for load path ③.

For the $-\sigma_{22} \rightarrow \gamma_{12}$ load path, results in a similar format are shown in Fig. 3. The shear responses with corresponding compression preloads are documented in the left column, while the increase in compressive strain caused by shear load is shown in the right column. One can generalise the insensitivity of the shear response to the compressive preload as

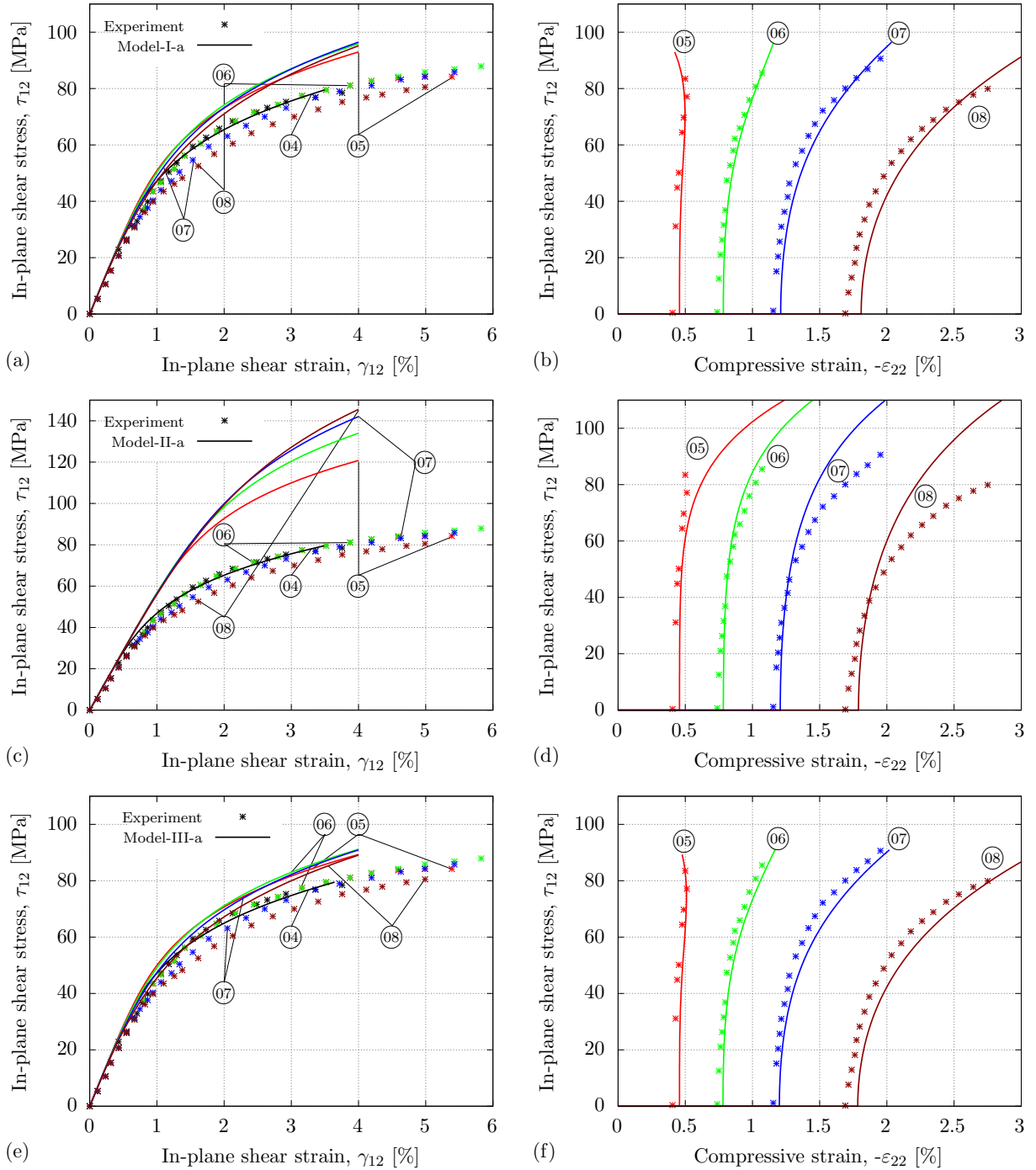


FIGURE 3: **Predictions for biaxial loads.** Comparison of the experimental and associative model responses for the $-\sigma_{22} \rightarrow \gamma_{12}$ loading path.

seen from the experimental data in the left column. Only at the highest compressive preload ($\textcircled{08}$), a small decrease in the shear stress is seen. The insensitivity can also be inferred from plots in the right column, where for load paths $\textcircled{05}$ and $\textcircled{06}$ only a small increase in the compressive strain is observed during shear load. Substantial increase is only seen for load paths $\textcircled{07}$ and $\textcircled{08}$). The predicted shear responses of Model-I-a do not agree well with experiments as seen in Fig. 3 (a). Owing to pressure-dependent plastic response functions, the transverse compression load hinders the onset of yielding and thus results in the reduced plastic flow [8]. Consequently, the shear response in presence of compression is over-predicted. Excellent agreement with experiments can be seen in Fig. 3 (b). Likewise, the shear response in presence of compression is over-predicted by Model-II-a in the $-\sigma_{22} \rightarrow \gamma_{12}$ load path, as seen in Fig. 3 (c). Good qualitative agreement is seen with the experimental response in Fig. 3 (d). Predictions of Model-III-a for the $-\sigma_{22} \rightarrow \gamma_{12}$ load path is shown in Fig. 3 (e) and (f). Figure 3 (e) depicts a comparison of the model predictions and experimental shear response in presence of compression, where a good conformity with experiments is seen. The predicted compressive strains are in excellent agreement with experiments which is evident from Fig. 3 (f).

5.2.2. Erroneous predictions of the associated flow response.

To illustrate erroneous predictions of the associated flow response, the shear dominated $\tau_{12} \rightarrow -\varepsilon_{22}$ load path is considered. The γ_{12} vs. $-\varepsilon_{22}$ strain response in Figure 4 (a), (c) and (e) shows Model-I-a, Model-II-a and Model-III-a predictions for the load paths $\textcircled{01}$ – $\textcircled{04}$. The assessment of the plastic flow direction is apparent in these plots. For a just shear stress state (load path $\textcircled{04}$), positive transverse strain is induced by Model-I-a and Model-III-a which is not expected (Figs. 4 (a) and (e)). The same phenomenon is observed for shear dominated combined stress states (load paths $\textcircled{01}$ – $\textcircled{03}$) where physically unrealistic transverse tensile strain is predicted. This aspect is also demonstrated in [8] for load paths $\textcircled{05}$ – $\textcircled{08}$ where the pressure-dependent model with an associative flow rule predicts a decrease in the transverse strain for an increasing shear strain, a trend opposite to the experimental results reported in [3]. For Model-II-a, it is seen that the direction of plastic flow is generally aligned to the vertical axis for just shear stress state, though a small amount of compressive strain is induced (Fig. 4 (c)), again which is unrealistic. The non-physical behaviour of associated flow response is also discussed in the recent work [30], with respect to compressive off-axis tests on a carbon-epoxy material. There, it is also seen that tensile rather than compressive transverse strain is predicted for 15° and 45° off-axis angles. This non-physical behaviour is a consequence of the negative slope of the Drucker-Prager-type yield surfaces used by these models, for just shear and shear dominated combined stress states. The corrected material response using a non-associative flow rule is shown in Fig. 4 (b), (d) and (e). In line with the expectations, it is seen that the direction of plastic flow is aligned to the vertical axis for just shear stress state. Additionally, the predicted transverse strains are compressive for shear dominated combined stress states. In what follows, predictions of the non-associative flow rule are reported and discussed based on the foregoing observations.

5.2.3. Predictions of the non-associated flow response.

Figure 5 (a) and (b) show a comparison of Model-I-b predictions and experimental responses for the $\tau_{12} \rightarrow -\varepsilon_{22}$ load path. The non-associative flow rule corrects the physically inconsistent material response exhibited by the associative flow rule under shear dominated loads, as seen in Fig. 5 (a). A good qualitative agreement with experiments is seen

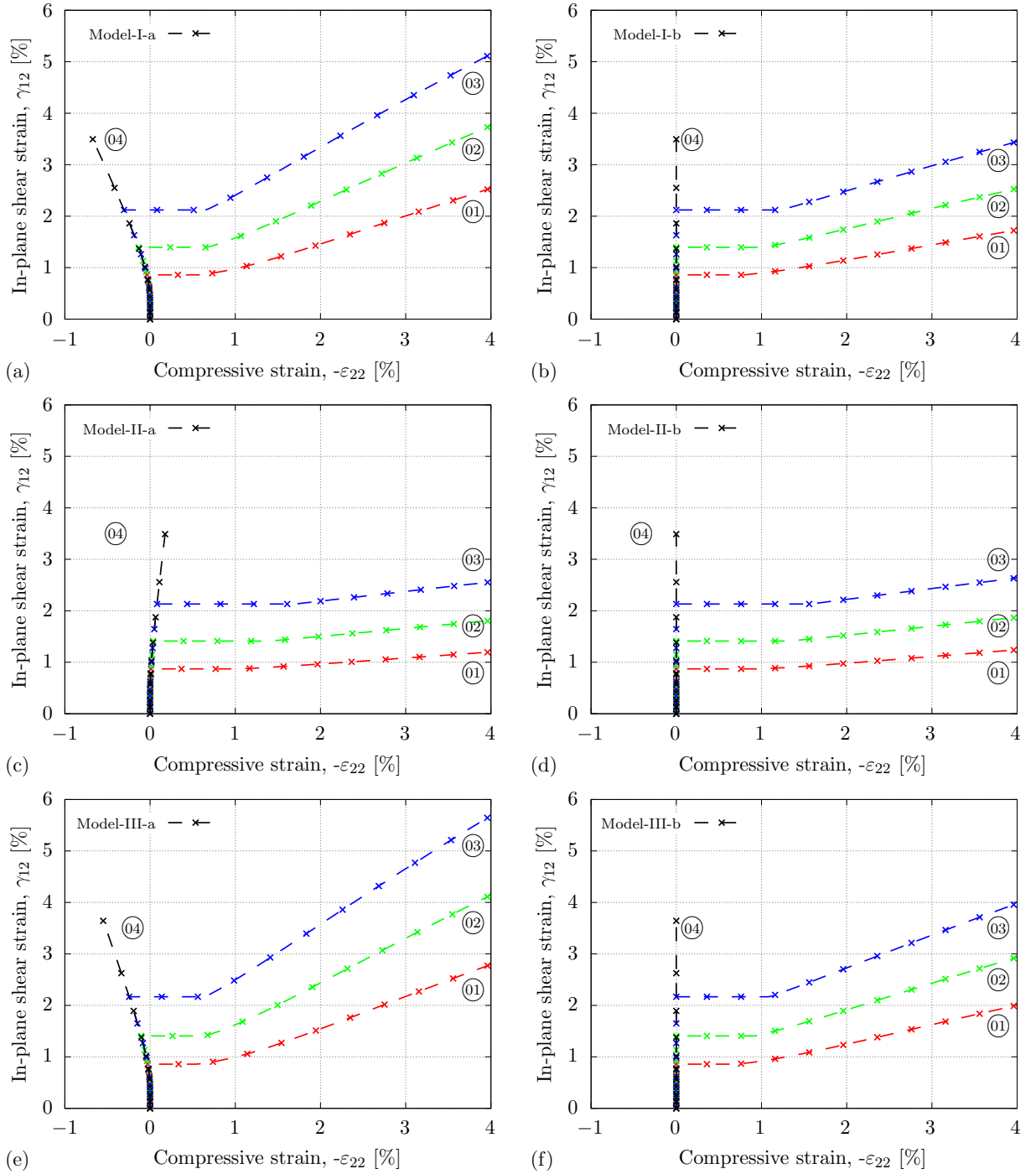


FIGURE 4: **Predictions for biaxial loads.** Erroneous predictions of the associated flow response and corrected response by the non-associative flow rule for shear dominated loads.

for the compressive response. In comparison with Model-I-a, the predicted shear strains are much lower, and significant deviations are observed for load paths ①–③ which is visible from Fig. 5 (b). Figure 5 (c) and (d) shows the Model-II-b model predictions for the $\tau_{12} \rightarrow -\epsilon_{22}$ load path. Predictions of the non-associative model are largely similar to that of the associative model (Model-II-a). Figure 5 (e) and (f) shows a comparison of Model-III-b predictions and the experimental results for the $\tau_{12} \rightarrow -\epsilon_{22}$ load path. The predicted compressive response by the model is in good agreement with experiments, as

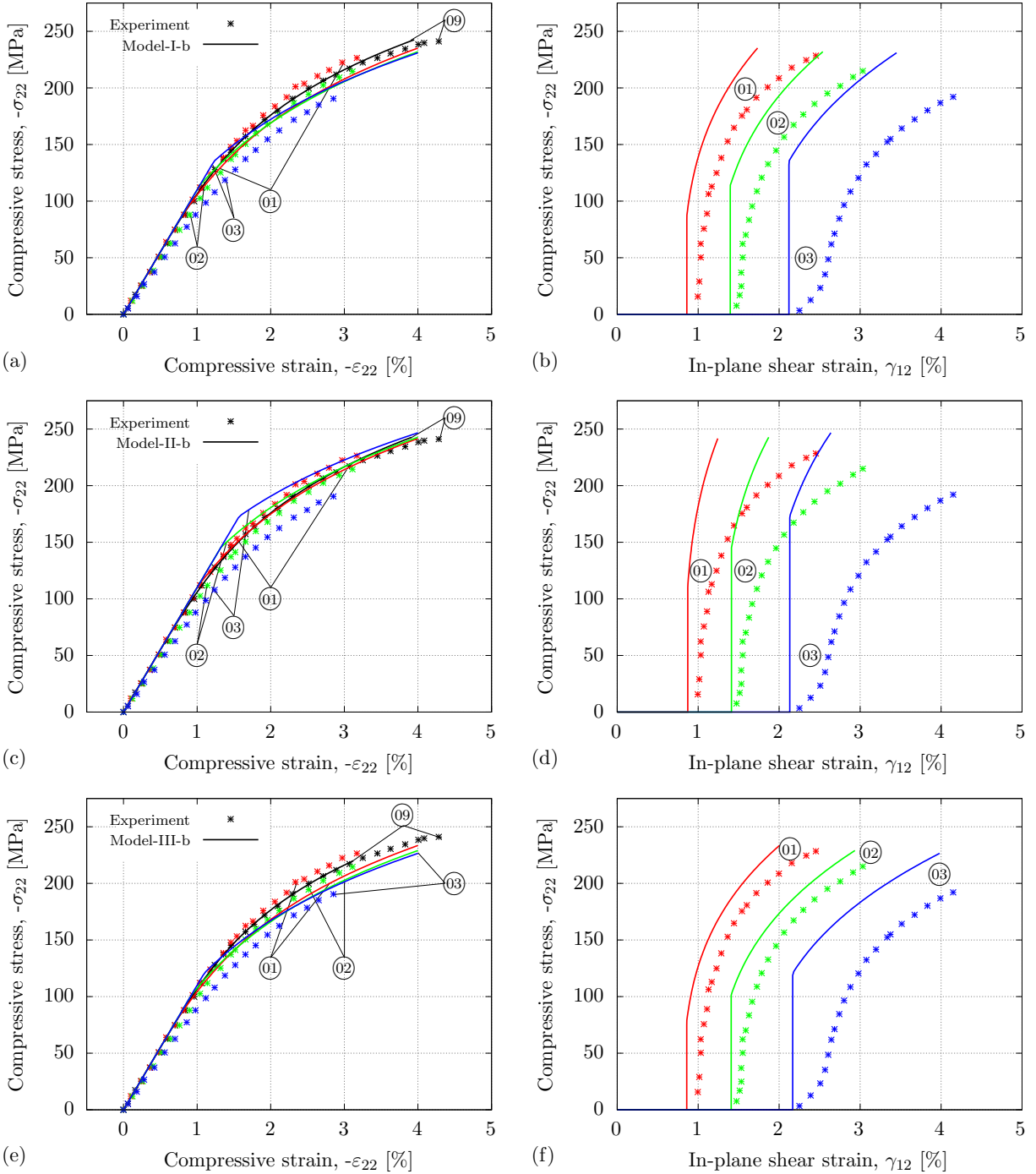


FIGURE 5: **Predictions for biaxial loads.** Comparison of the experimental and non-associative model responses for the $\tau_{12} \rightarrow -\varepsilon_{22}$ loading path.

seen in Fig. 5 (e). The predicted transverse strains are compressive for the load paths ①–④, thereby eliminating the inconsistencies exhibited by Model-III-a. Additionally, there is no over-prediction of transverse stress for load path ③. Good agreement with the experimental response is seen in Fig. 5 (f) in comparison with Figs. 5 (b) and (d).

Figure 6 shows non-associative models predictions for the $-\sigma_{22} \rightarrow \gamma_{12}$ load path. Similar to the associated flow response, the shear response in presence of compression is over-predicted by Model-I-b as seen in Fig. 6 (a). The compressive strains are also over-

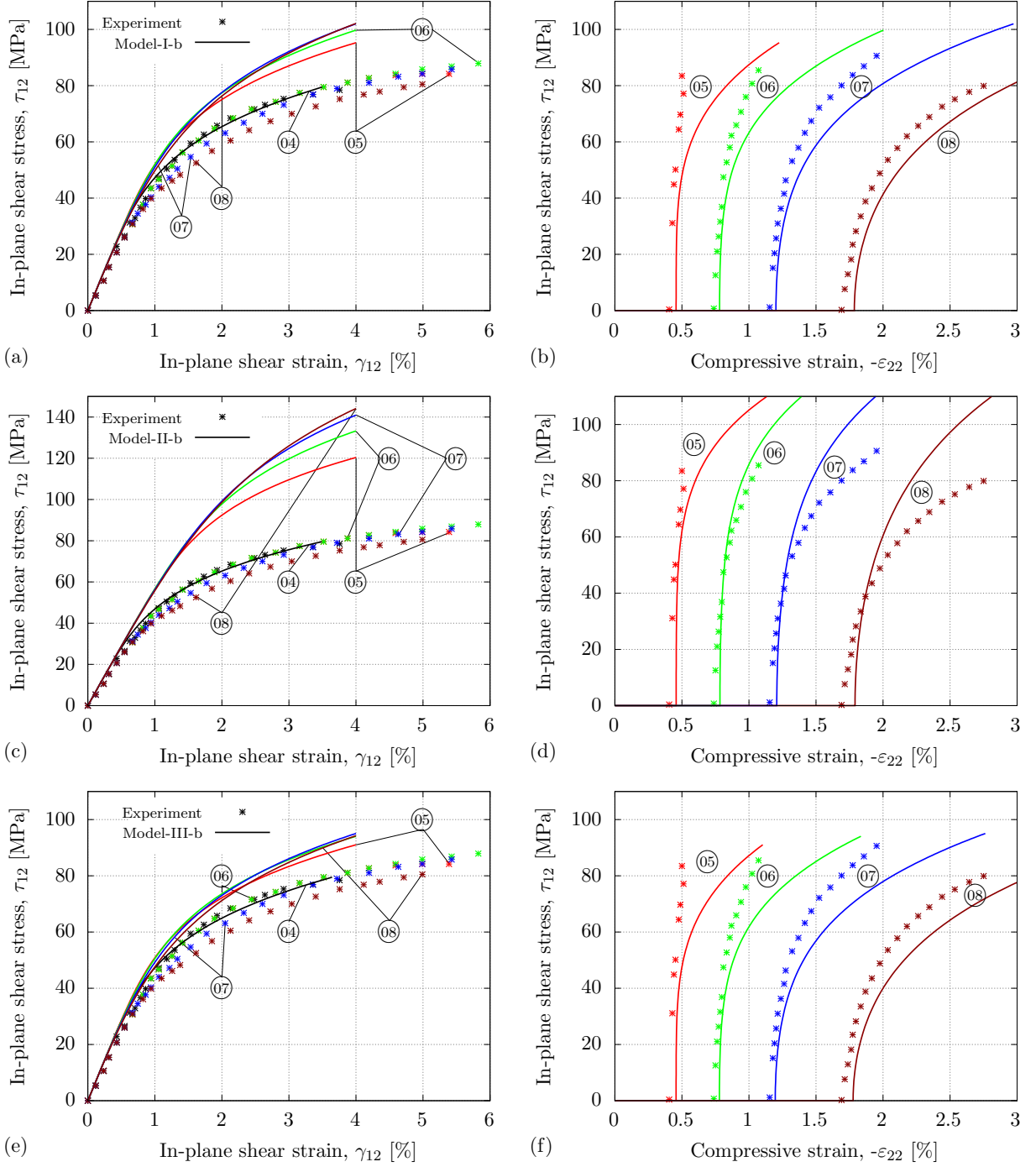


FIGURE 6: **Predictions for biaxial loads.** Comparison of the experimental and non-associative model responses for the $-\sigma_{22} \rightarrow \gamma_{12}$ loading path.

predicted for load paths (05)–(08). Figure 6 (c) and (d) shows Model-II-b predictions for the $-\sigma_{22} \rightarrow \gamma_{12}$ load path. Predictions of the non-associative model are largely similar to that of the associative model. Plots depicting Model-III-b predictions and experimental results for the $-\sigma_{22} \rightarrow \gamma_{12}$ load path are shown in Fig. 6 (e) and (f). The shear response in presence of compression is slightly over-predicted by the model as seen in Fig. 6 (e). This is a direct consequence of a higher value of the governing coefficient of hydrostatic pressure, as higher transverse stress leads to excessive stiffening in the shear response [8]. The parameter κ in Eqn. (38) should be rather low based on the experimental results where

shear responses of the load paths ④–⑦ are almost the same, see [3]. The predicted $-\varepsilon_{22}$ agrees well with the experimental results as seen in Fig. 6 (f) with slight overestimation for load path ⑧.

5.2.4. Discussion.

An assessment of Figs. 2, 3, 5 and 6 reveals that the predictions are in excellent agreement with the experimental results whilst using an associative flow rule. For the considered load paths, the compressive response with shear preload and shear response with compression preload is over-predicted by all the models, only at the highest value of the respective preload. It has been reported in [3] that the presence of shear preload does not affect the compressive response significantly. Likewise, the shear response is almost insensitive to the presence of compression preload. These aspects are also reflected in the model predictions. However, the associative flow rule exhibits non-physical constitutive response under shear dominated combined stress states as seen from Fig. 4. The non-associated flow response circumvents these physical inconsistencies and yields the expected behaviour, but notable deviations are observed for biaxial load paths where the shear response in presence of compression is overestimated. A possible explanation could be the influence of dilatation on the plastic deformation due to crazing [59,60]. In this case, the plastic flow potential needs to be reformulated such that it is pressure dependent but stress free in the fibre direction. A comprehensive discussion is beyond the scope of the present work as it is unknown if crazing was observed in the tests considered here.

6. Conclusions.

In this work, the effect of isotropic and anisotropic yield functions in conjunction with associative and non-associative flow rules on the non-linear inelastic behaviour of polymeric composites is investigated. Three different plastic response functions (Model-I, Model-II and Model-III) are considered. All the models are first calibrated to reproduce the experimental pure shear and compression response. The calibrated models are evaluated in detail by comparison to experimental data for a range of bi-axial loads. The reported predictions show a high degree of conformance with the experimental response.

The experimental investigations are affirmative to the fact that to realistically predict the non-linear behaviour of polymeric composite materials for different load combinations, the constitutive response must be pressure sensitive. Further, plastic response functions that are pressure-dependent but isotropic, need to be either mathematically manipulated [61,62] or extended to anisotropic forms [16,28] to reproduce the experimentally observed biaxial response. It should also be emphasised here, that the models based on the concept of mapped tensors [18,19] do not fully ensure a linear elastic fibre response owing to singularity problems of the transformation tensor. Clearly, the stress tensor should be decomposed not just into volumetric and deviatoric components, but also into the respective normal and shear modes associated with the symmetry group. Only then can the experimental biaxial response be captured accurately on the meso scale. Additionally, it can be inferred that although both associative and non-associative flow rules capture certain aspects of the polymeric composites, they do not reproduce the full complexity. The non-associative flow rule circumvents the physical inconsistencies induced by the associated flow response under shear dominated combined stress states, and yields the expected behaviour. However, notable deviations are observed for the considered load paths where the shear response in presence of compression is overestimated. This can

be attributed to the choice of a pressure-independent plastic flow potential (thereby a pressure-independent flow rule) and a rate-independent setting, as a result of which the predicted transverse strains are much higher than those observed experimentally. At this point, the choice of a flow rule is unclear and would require additional experimental data for bi-axial responses, such as $\tau_{12} \rightarrow -\sigma_{22}$ which denotes the evolution of yield surface and plastic flow potential. One can then use the proposed associative or non-associative plasticity models for a wide range of loading scenarios.

References

- [1] Weeks, C.A. and Sun, C.T. [1995]: “Nonlinear Rate Dependence of Thick-Section Composite Laminates. High Strain Rate Effects on Polymer, Metal and Ceramic Matrix Composites and Other Advanced Materials”. *Y.D.S. Rajapakse and J.R. Vinson, eds., ASME*, 48: 81–95.
- [2] Vogler, T.J. and Kyriakides, S. [1998]: “On the effect of loading rate on the compressive strength of an AS4/PEEK composite”. *Journal of Applied Mechanics, ASME*, 65: 1056–1058.
- [3] Vogler, T.J. and Kyriakides, S. [1999]: “Inelastic behavior of an AS4/PEEK composite under combined transverse compression and shear. Part I: experiments”. *International Journal of Plasticity*, 15: 783–806.
- [4] G’sell, C., Jacques, D. and Favre, J.P. [1990]: “Plastic behavior under simple shear of thermosetting resins for fiber composite matrices”. *Journal of material sciences*, 25: 2004–2010.
- [5] Gilat, A., Goldberg, R.K. and Roberts, G.D. [2005]: “Strain rate sensitivity of epoxy resin in tensile and shear loading”. Technical report, TM-2005-213595.
- [6] Schuecker, C. and Pettermann, H.E. [2008]: “Combining elastic brittle damage with plasticity to model the non-linear behavior of fiber reinforced laminates”. *Computer methods in applied sciences*, 10: 99–117.
- [7] Pettermann, H.E., Planskensteiner, A.F., Böhm, H.J. and Rammerstorfer, F.J. [1993]: “A thermo-elasto-plastic constitutive material law based on an incremental Mori-Tanaka approach”. *Computers and Structures*, 71: 197–214.
- [8] Hsu, S.-Y., Vogler, T.J. and Kyriakides, S. [1999]: “Inelastic behavior of an AS4/PEEK composite under combined transverse compression and shear. Part II: modeling”. *International Journal of Plasticity*, 15: 807–836.
- [9] Doghri, I. and Ouaar, A. [2003]: “Homogenization of two-phase elasto-plastic composite materials and structures. Study of tangent operators, cyclic plasticity and numerical algorithms”. *International Journal of Solids and Structures*, 40: 1681–1712.
- [10] Doghri, I., Adam, L. and Bilger, N. [2010]: “Mean-field homogenization of elasto-viscoplastic composites based on a general incrementally affine linearization method”. *International Journal of Plasticity*, 26(2): 219–238.
- [11] Hill, R. [1950]: “The mathematical theory of plasticity”. Oxford: clarendon press.

- [12] Barlat, F., Lege, D.J. and Brem, D.J. [1991]: “A six-component yield function for anisotropic materials”. *International Journal of Plasticity*, 5: 693–712.
- [13] Voyiadjis, G.Z. and Thiagarajan, G. [1995]: “An anisotropic yield surface model for directionally reinforced metal-matrix composites”. *International Journal of Plasticity*, 11: 867–894.
- [14] Barlat, F., Aretz, H., Yoon, J.W., Karabin, M.E., Brem, J.C. and Dick, R.E. [2005]: “Linear transformation-based anisotropic yield functions”. *International Journal of Plasticity*, 21: 1009–1039.
- [15] Smith, J., Liu, W.K. and Cao, J. [2015]: “A general anisotropic yield criterion for pressure-dependent materials”. *International Journal of Plasticity*, 75: 2–21.
- [16] Nagaraja, S.G., Pletz, M. and Schuecker, C. [2019]: “Constitutive modeling of anisotropic plasticity with application to fiber-reinforced composites”. *International Journal of Solids and Structures*, 180-181: 84–96.
- [17] Nagaraja, S.G. and Schuecker, C. [2019]: “On the formulation of anisotropic plasticity for polymeric composites–rate-dependent models with non-linear isotropic/kinematic hardening”. In *Proceedings in Applied Mathematics and Mechanics*.
- [18] Car, E., Oller, S. and Oñate, E. [2000]: “An anisotropic elastoplastic constitutive model for large strain analysis of fiber reinforced composite materials”. *Computer methods in applied mechanics and engineering*, 185: 245–277.
- [19] Car, E., Oller, S. and Oñate, E. [2001]: “A large strain plasticity model for anisotropic materials-composite material application”. *International Journal of Plasticity*, 17: 1437–1463.
- [20] Sun, C.T. and Chen, J.L. [1989]: “A simple flow rule for characterizing nonlinear behavior of fiber composite”. *Journal of Composite Materials*, 23: 1009–1020.
- [21] Chen, J.L. and Sun, C.T. [1993]: “A plastic potential function suitable for anisotropic fiber composites”. *Journal of Composite Materials*, 27: 1379–1390.
- [22] Xie, M. and Adams, D.F. [1995]: “A plasticity model for unidirectional composite materials and its applications in modeling composites testing”. *Composites Science and Technology*, 27: 11–21.
- [23] Rogers, T. [1987]: “Yield criteria, flow rules and hardening in anisotropic plasticity”. *Boehler, Yielding, damage and failure of anisotropic solids, EGF publication*, 5: 53–79.
- [24] Spencer, A.J.M. [1992]: “Plasticity theory for fibre-reinforced composites”. *Journal of Engineering Mathematics*, 26: 107–118.
- [25] Tsai, J. and Sun, C.T. [2002]: “Constitutive model for high strain rate response of polymeric composites”. *Composites Science and Technology*, 62(10): 1289–1297.
- [26] Kontou, E. and Spathis, G. [2006]: “Application of finite strain viscoplasticity to polymeric fiber composites”. *International Journal of Plasticity*, 22(7): 1287–1303.
- [27] Vyas, G.M., Pinho, S.T. and Robinson, P. [2011]: “Constitutive modeling of unidirectional composites at the ply level using a plasticity-based approach”. *Composite Science and Technology*, 78: 1068–1074.

- [28] Vogler, M., Rolfes, R. and Camanho, P.P. [2013]: “Modeling the inelastic deformation and fracture of polymer composites - Part I: Plasticity model”. *Mechanics of Materials*, 59: 50–64.
- [29] Miehe, C. [1998]: “A constitutive frame of elastoplasticity at large strains based on the notion of a plastic metric”. *International Journal of Solids and Structures*, 35: 3859–3897.
- [30] Laux, T., Gan, K.W., Dulieu-Barton, J.M. and Thomsen, O.T. [2019]: “A simple nonlinear constitutive model based on non-associative plasticity for UD composites: Development and calibration using a Modified Arcan Fixture”. *International Journal of Solids and Structures*, 162: 135–147.
- [31] Mosler, J. and Bruhns, O.T. [2009]: “Towards variational constitutive updates for non-associative plasticity models at finite strain: Models based on a volumetric-deviatoric split”. *International Journal of Solids and Structures*, 46: 1676–1684.
- [32] Papadopoulos, P. and Taylor, R.L [1994]: “On the application of multi-step integration methods to infinitesimal elastoplasticity”. *International Journal for Numerical Methods in Engineering*, 37: 3169–3184.
- [33] Simó, J.C. and Hughes, T.J.R. [2000]: “Computational Inelasticity”. Mechanics and Materials, Springer.
- [34] Coleman, B.D. and Noll, W. [1963]: “The thermodynamics of elastic materials with heat conduction and viscosity”. *Archive for Rational Mechanics and Analysis*, 13: 167–178.
- [35] Coleman, B.D. and Gurtin, M.E. [1967]: “Thermodynamics with Internal State Variables”. *The Journal of Chemical Physics*, 47(2): 597–613.
- [36] Lubliner, J. [1997]: “Plasticity theory”. Maxwell Macmillan International Edition.
- [37] Khan, A.S. and Huang, S. [1995]: “Continuum Theory of Plasticity”. A Wiley-Interscience Publication, John Wiley and Sons, New York.
- [38] Aldakheel, F. and Miehe, C. [2017]: “Coupled Thermomechanical response of gradient plasticity”. *International Journal of Plasticity*, 91: 1–24.
- [39] Perzyna, P. [1971]: “Thermodynamics of rheological materials with internal changes”. *Journal de Mécanique*, 10: 391–408.
- [40] Lubliner, J. [1972]: “On the thermodynamic formulations of non-linear solid mechanics”. *International Journal of Non-linear Mechanics*, 7: 237–254.
- [41] Miehe, C., Apel, N. and Lambrecht, M. [2002]: “Anisotropic additive plasticity in the logarithmic strain space: modular kinematic formulation and implementation based on incremental minimization principles for standard materials”. *Computer methods in applied mechanics and engineering*, 191: 5383–5425.
- [42] Boehler, J.P. [1979]: “A simple derivation of representations for non-polynomial constitutive equations in some case of anisotropy”. *ZAMM*, 59: 157–167.
- [43] Lu, J. and Zhang, L. [2005]: “Physically motivated invariant formulation for transversely isotropic hyperelasticity”. *International Journal of Solids and Structures*, 42: 6015–6031.
- [44] Liu, I.-S. [1982]: “On representations of anisotropic invariants”. *International journal of engineering sciences*, 31: 1099–1109.

- [45] Zheng, Q.S. and Spencer, A.J.M. [1993]: “Tensors which characterize anisotropies”. *International journal of engineering sciences*, 31 (4): 679–693.
- [46] Zheng, Q.S. [1994]: “Theory of representations for tensor functions—a unified invariant approach to constitutive equations”. *Applied mechanics review*, 47 (11): 545–586.
- [47] Smith, G.F. [1965]: “On isotropic integrity bases”. *Archive for Rational Mechanics and Analysis*, 18: 282–292.
- [48] Spencer, A.J.M. [1971]: “Theory of invariants”. *Continuum Physics, Academic Press, New York*, 1: 239–353.
- [49] Spencer, A.J.M. [1987]: “Isotropic Polynomial Invariants and Tensor Functions”. Boehler, Applications of Tensor Functions in Solid Mechanics, CISM course No. 292, Springer-Verlag, Wien.
- [50] Schröder, J., Gruttmann, F. and Löblein, J. [2002]: “A simple orthotropic finite elasto-plasticity model based on generalized stress-strain measures”. *Computational Mechanics*, 30: 48–64.
- [51] Papadopoulos, P. and Lu, J. [2001]: “On the formulation and numerical solution of problems in anisotropic finite plasticity”. *Computer Methods in Applied Mechanics and Engineering*, 190: 4889–4910.
- [52] Naghdi, P.M. and Trapp, J.A. [1975]: “The significance of formulating plasticity theory with reference to loading surfaces in strain space”. *International Journal of Engineering Sciences*, 13: 785–797.
- [53] Naghdi, P.M. and Trapp, J.A. [1975]: “Restrictions on constitutive equations of finitely deformed elastic-plastic materials”. *Quarterly Journal of Mechanics and Applied Mathematics*, 28: 25–46.
- [54] Casey, J. [1984]: “A simple proof of a result in finite plasticity”. *Quarterly Applied Mathematics*, 42: 61–71.
- [55] Voyiadjis, G.Z. and Thiagarajan, G. [1996]: “A cyclic anisotropic-plasticity model for metal-matrix composites”. *International Journal of Plasticity*, 12: 69–91.
- [56] Armstrong, P.J. and Frederick, C.O. [1996]: “A mathematical representation of multiaxial Bauschinger effect”. CEBG Report, RD/B/N/731, Berkeley Laboratories, R and D Department, CA.
- [57] Prager, W. [1956]: “A new method of analyzing stresses and strains in work-hardening plastic solids”. *Journal of Applied Mechanics, ASME*, 23: 493–496.
- [58] “ABAQUS/Standard User’s Manual, Version 6.13-2”. Dassault Systemès Simulia Corp., Providence, RI, USA.
- [59] Chen, F., Gatea, S., Ou, H., Lu, B. and Long, H. [2016]: “Fracture characteristics of PEEK at various stress triaxialities”. *Journal of the Mechanical Behavior of Biomedical Materials*, 64: 173–186.
- [60] Zaïri, F., Naït-Abdelaziz, M., Gloaguen, J.M. and Lefebvre, J.M. [2008]: “Modelling of the elasto-viscoplastic damage behaviour of glassy polymers”. *International Journal of Plasticity*, 24(6): 945–965.
- [61] Raghava, R., Caddell, R.M. and Yeh, G.S.Y [1973]: “The macroscopic yield behaviour of polymers”. *Journal of Materials Science*, 8(2): 225–232.

- [62] Zhang, J., Kikuchi, V., Li, V., Yee, A. and Nusholtz, G. [1998]: “Constitutive modeling of polymeric foam material subjected to dynamic crash loading”. *International Journal of Impact Engineering*, 21(5): 369–386.